EMT Model of 20-MW Wind Generator for Real-time Simulation of HVDC Networks

Das, Dwijasish; Rueda-Torres, José-Luis

DOI
10.1016/j.ifacol.2024.07.545

Publication date
2024

Document Version
Final published version

Published in
IFAC-PapersOnLine

Available online at www.sciencedirect.com

ScienceDirect

IFAC PapersOnline CONFERENCE PAPER ARCHIVE

IFAC PapersOnLine 58-13 (2024) 581–586

EMT Model of 20-MW Wind Generator for Real-time Simulation of HVDC Networks

Dwijasish Das * **José-Luis Rueda-Torres** *

* *Delft University of Technology (TU Delft), Delft, Netherlands (e-mails: d.das-1@tudelft.nl, j.l.ruedatorres@tudelft.nl).*

Abstract: As modern trends demand efficient methods to massively and promptly exploit clean energy, there is an urgent need of solutions that can help the ambition of accelerating the development and integration of larger scale energy systems with the capacity to extract, store, and utilize huge amounts of renewable energy sources. In view of this, the rated power output of the wind generation technology is expected to significantly increase in the near future to enable multi-gigawatt roll outs, e.g. the European plans for offshore infrastructure development in the North-Sea. Besides, gigantic energy systems shall transmit the power to onshore interconnected systems via HVDC transmission. This paper introduces an EMT model of a 20 MW wind generation system with the conventional back-to-back converter replaced by a combination of an AC to DC converter and a DC to DC converter. While the need of such systems is acknowledged in the literature, the design and performance analysis of high power implementation of such systems have not been addressed yet. The proposed system operates at a voltage level of 100 kV, which can directly transfer power through HVDC interconnection. The designed control aspects are outlined and the resulting dynamic response obtained from real-time digital simulation (RTDS) are discussed. The presented wind generator concept can help in reducing the size of a planned energy system by requiring lesser system components. Also, the system efficiency can be enhanced by decreasing the number of power conversion stages.

Keywords: EMT model, HVDC transmission system, high-power dual active bridge converter, large-scale energy systems, real-time digital simulation, wind generator.

1. INTRODUCTION

With the global interest of power generation shifting towards renewal energy sources (RES), technologies associated with solar power and wind power have seen significant developments. Wind energy is seen as a source with the highest potential to deliver large amounts of power to interconnected electrical power systems Beig and Muyeen (2016). While wind generation systems can be located either onshore or offshore, offshore system developments are pursuing an accelerated development due to potential of achieving multi-gigawatt scale and also due to steadier wind speeds and the absence of land space related limitations Fennell (2018). For instance, owing to the tremendous wind energy potential in the North Sea region, the surrounding countries like Denmark, Germany and the Netherlands are exploring the scope of developing the North Sea Wind Power Hub (NSWPH) Misyris et al. (2020). Such projects demand the installation of high-power wind generation systems to ensure the maximum harnessing of available wind energy resource. ENTSO-E (Jan., 2024) highlights various transmission system needs for such offshore systems.

The power rating of a single wind generator is growing at a very high rate with time Yuan et al. (2022). With the increase in blade length and swept area, higher wind power can be captured. Currently, the world's largest operating wind generator is located in Fujian, China with a power rating of 16 MW Blain (2023). There are attempts to go even higher with the power levels. Companies like MingYang and CSSC Haizhuang are already working on the concepts of massive 18 MW wind generators Nehls (2023). In Sweden, there are ongoing plans to have gigawatt scale wind power plants with 20 MW generators Richard (2021). In the literature, researchers have discussed the possibilities of even higher power wind generators going up to 30 MW Yuan et al. (2022); Proctor (2023).

With the increase in power ratings of the wind generators, the voltage ratings also need to rise Poynter (2021). Wind generators upto 8 MW are seen to have a voltage level of 690 V Pow. Nevertheless, as the power levels rise further, the voltage levels of the generator system need to rise such that the overall currents are within the limits. Thus, medium voltage converters are the preferred solutions for such high power wind generation systems, to ensure size reduction, weight reduction and also to reduce component count Yuan (2014).

Another paradigm shift researchers are currently eyeing in the wind energy sector is the feasibility of DC collection from off-shore wind energy systems Chuangpishit et al.

⋆ The research work shown in this paper has received funding from Shell Global Solutions International B.V. It reflects only the authors' views, and the above indicated organization is not responsible for any use that may be made of the information it contains in.

10.1016/j.ifacol.2024.07.545

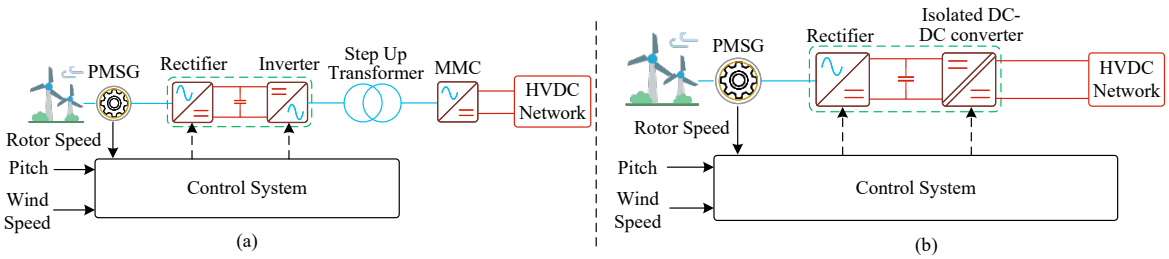

Fig. 1. (a) Conventional PMSM wind generator system. (b) Proposed PMSM wind generator system with HVDC output.

(2014); De Prada Gil et al. (2015). Since off-shore wind power is generally transmitted with HVDC transmission systems Ryndzionek and Sienkiewicz (2020), a DC collection helps in reduction of power conversion stages. The conventional wind generation system extracts power with a back-to-back AC-DC-AC conversion process. There have been studies to incorporate changes in this structure to make it more suitable for DC systems. In Guan (2019), a wind power plant based on isolated DC-DC converters is proposed and connection to HVDC network is achieved with series cascading of multiple converters. However, such a configuration is not suitable for very large wind generators with power ratings of tens of mega watts. In Li et al. (2023), DC wind generators are analyzed for grid side transient faults. Non isolated cascaded DC-DC converters are considered in the study.

While researchers are turning towards DC wind generators for various advantages, there exists a major technology gap in the field of DC-DC power conversion that needs to be addressed before high power DC collection can become a reality Follo et al. (2021). Moreover, there is tremendous scope of the isolated DC-DC converter for such application and that is another area that has not been explored much. This paper presents a model of a 20 MW wind generation system, built by using the RSCAD software package for real-time digital simulation (RTDS), where the nacelle is composed of an AC-DC and an isolated DC-DC converter instead of the conventional back-to-back converter. The presented system can be part of a network of similar off-shore wind generator, which can collectively inject DC power into a HVDC network for transmission from off-shore to on-shore locations. The paper is organized as follows. Section 2 offers a description of the proposed PMSG wind generation electrical system, Section 3 explains the details of the overall control. Section 4 presents the simulation, results and the paper is concluded in Section 5.

2. DESCRIPTION OF THE PROPOSED PMSM WIND GENERATION SYSTEM

A conventional wind generation system with back-to-back converter is shown in Fig. 1(a) Honarbari et al. (2021). The wind energy drives the turbine which is coupled to the generator. Electric power produced by the generator is converted by the AC-DC converter also known as the machine side converter (MSC). The DC power is again converter to AC with the DC-AC converter known as the grid side converter (GSC). The AC power obtained from the GSC is step-up to a higher voltage level typically from around 2 kV to 33 kV or 66 kV. For HVDC transmission systems, the power is again converter to HVDC with the help of modular multi-level converters (MMC) and finally fed to the HVDC network.

Fig. 1(b) shows the proposed configuration. The generator is rated at a voltage level of 3.3 kV line-to-line. The MSC acts as a controlled rectifier and converts the AC power to DC. This DC bus is maintained at a voltage level of 6 kV by the subsequent stage. An isolated DC-DC converter forms the second stage of the conversion process. This is the GSC for the proposed power conversion system. In addition to maintaining the 6 kV DC bus voltage, the isolated DC-DC converter also steps-up the DC form 6 kV to 100 kV and injects power into the 100 kV HVDC network. DC transmission links ranging from 100 kV to 800 kV are generally classified as HVDC transmission links Shepard (2020). The world's first HVDC transmission system was rated at 100 kV and 20 MW Tiku (2014). Current HVDC trends indicate operation at voltage levels ranging from 325kV DC to 525 kV ENTSO-E (2024). There are limited research available for the dual active bridge converter operating at such voltage levels. Consequently, for the preliminary investigations, the lower threshold voltage for HVDC transmission is being considered in this paper. Additionally, to handle such high voltage, multiple power electronic switches are needed in each branch of the H-bridges. However, for the sake of simplicity, an individual switch is used in each branch.

The isolated DC-DC converter comprises of two bridges - primary and the secondary. These bridges are interfaced with a medium frequency transformer Rik W. DeDoncker (1989). The primary bridge converts the DC input into a pulsed AC waveform. Based on the turns ratio of the transformer, the voltage transformation is achieved which changes the magnitude of the pulsed AC voltage available at the secondary side. The secondary bridge converts the pulsed AC into DC. The voltage transformation achieved at this stage helps eliminate the conventional step-up transformer. Moreover, as the power is obtained in the form of DC, further power conversion stage is not necessary for HVDC transmission.

3. DETAILS OF OVERALL CONTROL

The wind turbine is rotated by the flow of wind and the wind energy is converted to electrical energy by a permanent magnet synchronous generator (PMSG) into three phase AC power. This power is conditioned to be fed to the grid with the help of two main power electronic converter - the MSC or the rectifier and the GSC which is the isolated DC-DC converter. Fig. 2 shows the detailed circuit diagrams of these power electronic converters. The converters are controlled by developing firing pulses for

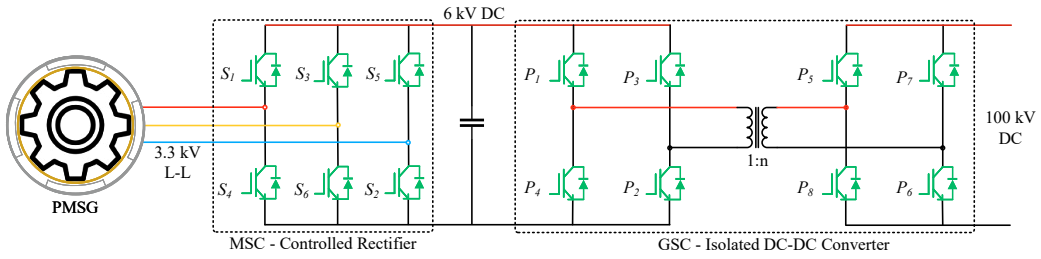

Fig. 2. Circuit diagram of the power electronic converters in the proposed system.

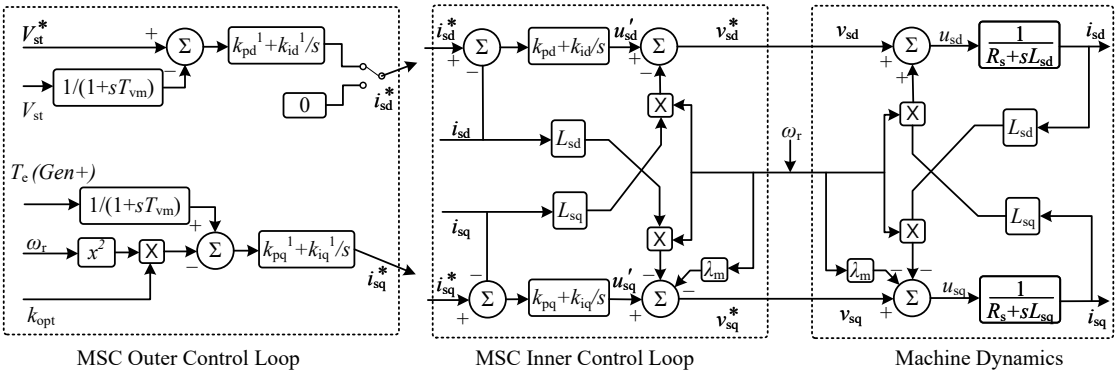

Fig. 3. Control diagram of machine side converter.

the switches based on desired manner of operation. The detailed operation and controlling action generated for these two converters are discussed as follows.

3.1 Machine Side Converter - Rectifier

In the proposed energy conversion system, the MSC converts the AC power to DC. This converter is also responsible for extracting maximum power from the wind turbines by controlling the electrical torque. To maintain the maximum power, this converter is operated in current control mode and thus reference currents need to be generated. The control diagram of the MSC is shown in Fig. 3. The converter receives the AC power from the stator of the PMSG. By controlling the quadrature axis stator current, the machine electrical torque can be controlled.

The power output of a wind generator is proportional to the cube of the wind speed Kusiak et al. (2009). The maximum power output can be expressed as a function of the turbine rotor speed as follows.

$$P_{out} = k_{opt}\omega_r^3 \tag{1}$$

where, k_{opt} is the optimal coefficient for maximum possible turbine power and ω_r is the rotational speed of the wind turbine.

Thus the maximum mechanical torque is expressed as

$$T_{out} = k_{opt}\omega_r^2 \tag{2}$$

For the MSC outer loop control, the measured torque is subtracted from the torque reference and the error is fed to a proportional integral (PI) controller to control the quadrature axis stator current (i^*_{sq}). The stator terminal voltage (V_{st}) can also be controlled in a similar manner if necessary. The first section of Fig. 3 shows the MSC outer control loop.

The stator voltage equations can be written as follows.

$$\frac{d\boldsymbol{\lambda_s}}{dt} = \boldsymbol{v_s} + R_s\boldsymbol{i_s} \tag{3}$$

where, $\boldsymbol{\lambda_s}$, $\boldsymbol{v_s}$ and $\boldsymbol{i_s}$ are the phasors for the stator flux linkage, stator terminal voltage and stator winding current, respectively. R_s is the winding resistance of the stator.

The flux linkage for the stator can be expressed as

$$\boldsymbol{\lambda_s} = L_s\boldsymbol{i_s} + \lambda_m e^{j\theta_r}. \tag{4}$$

Here, L_s is the stator inductance expresses as the difference between the stator self inductance (L_{ss}) and mutual inductance (M_{ss}). λ_m is the maximum flux of the permanent magnet in the rotor and θ_r is the rotor angle.

Using (4) in (3), we get,

$$L_s\frac{d\boldsymbol{i_s}}{dt} = \boldsymbol{v_s} - R_s\boldsymbol{i_s} - j\omega_r\lambda_m e^{j\theta_r} \tag{5}$$

In the dq axis domain,

$$\begin{aligned}\boldsymbol{i_s} &= e^{j\theta_r}i_{sdq}\\ \boldsymbol{v_s} &= e^{j\theta_r}v_{sdq}\end{aligned} \tag{6}$$

Using (6) in (5), we get,

$$L_s\frac{di_{sdq}}{dt} + R_s i_{sdq} = v_{sdq} - j\omega_r L_s i_{sdq} - j\omega_r\lambda_m \tag{7}$$

The right hand side of (7) can be expressed as $\boldsymbol{u_{sdq}}$. Thus, the PMSG dynamics can be expressed as the following in d-q frame of reference.

$$\begin{aligned}L_s\frac{di_{sd}}{dt} + R_s i_{sd} &= u_{sd}\\ L_s\frac{di_{sq}}{dt} + R_s i_{sq} &= u_{sq}\end{aligned} \tag{8}$$

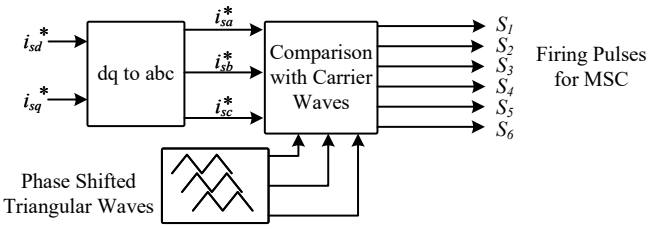

Fig. 4. Firing pulse generation for MSC.

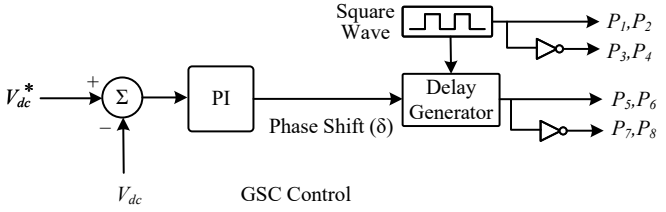

Fig. 5. Control block diagram for the isolated DC-DC converter.

where,

$$\begin{aligned} u_{sd} &= v_{sd} + \omega_r L_s i_{sq} \\ u_{sq} &= v_{sq} - \omega_r L_s i_{sd} - \omega_r \lambda_m \end{aligned} \tag{9}$$

The reference terminal voltages can be considered equal to the actual terminal voltages. This can be expressed as

$$\begin{aligned} v_{sd}^* &= v_{sd} \\ v_{sq}^* &= v_{sq} \end{aligned} \tag{10}$$

The machine dynamics can be represented with PI controllers as follows.

$$\begin{aligned} u_{sd}^{'} &= \left(k_{pd} + \frac{k_{id}}{s}\right).\Delta i_{sd} \\ u_{sq}^{'} &= \left(k_{pq} + \frac{k_{iq}}{s}\right).\Delta i_{sq} \end{aligned} \tag{11}$$

The inner control loop of the machine can be expressed as follows.

$$\begin{aligned} v_{sd}^* &= u_{sd}^{'} - \omega_r L_s i_{sq} \\ v_{sq}^* &= u_{sq}^{'} + \omega_r L_s i_{sd} + \omega_r \lambda_m \end{aligned} \tag{12}$$

The equations (11) and (12) respectively represent the MSC inner control loop and machine dynamics which are represented in the block diagram in Fig. 3.

The control block diagram in Fig. 3 show the generation of d-q axis stator currents for extracting maximum power from the PMSG. These are converted to abc axis to obtain the modulation signals for the MSC. Once these are obtained, they are compared with a triangular carrier wave of desired frequency to generate the switching pulses ($S_1 - S_6$) for the converter. The block diagram for firing pulse generation is shown in Fig. 4.

3.2 Grid Side Converter - Isolated DC-DC converter

The isolated DC-DC converter feeds the available power to the HVDC grid. The power flow equation of this converter is expressed as follows Rodríguez et al. (2015).

$$P_{DC-DC} = \frac{n\delta(1-\delta)V_{DC}V_{HVDC}}{2f_{GSC}L_{DC-DC}} \tag{13}$$

Table 1. Simulation Parameters

Parameters	Values
Rated turbine power	20 MW
Rated wind speed	12 m/s
Rated generator voltage	3.3 kV
DC link voltage	6 kV
HVDC grid voltage	100 kV
MSC switching frequency (f_{MSC})	2 kHz
GSC switching frequency (f_{GSC})	5 kHz

where, n is the turns ratio of the isolation transformer, δ is the firing angle delay between the primary and secondary side bridges of the isolated DC-DC converter, V_{DC} is the voltage of the common dc link between the MSC and the GSC, V_{HVDC} is the HVDC grid voltage. f_{GSC} represents the switching frequency and L_{DC-DC} is the isolation transformer inductance of the isolated DC-DC converter.

In the proposed system, the isolated DC-DC converter is used to maintain the common DC link voltage of the MSC and the GSC. Since the MSC is controlled to feed in the maximum available power DC link, this power is automatically transferred to the HVDC grid through the isolated DC-DC converter when the converter operates to maintain the common DC link voltage.

To maintain the common DC link voltage, the reference voltage is subtracted from the the actual voltage and the error is fed to a PI controller. This PI controller generates the delay (δ) that has to be set between the firing pulses of the primary and secondary side bridges. Switches P_1 and P_2 get the firing pulses from a square wave generator and P_3 and P_4 get the inverted pulses. Switches P_5 - P_8 get similar pulses respectively, with delay of δ. The control diagram is given in Fig. 5.

4. SIMULATION RESULTS

The proposed system is developed in RSCAD and simulated on a real time digital simulator (RTDS). The parameters used for the simulation are given in Table 1. The MSC and GSC switching frequencies are chosen such that there is a balance between the switching losses and cost at the power level of 20 MW, based on examples from literature. The isolated DC-DC converter is operated at a higher frequency to achieve better control performance with high voltage transformation ratios.

The wind generator model available in RSCAD FX2.0 library is used to represent the wind generator. The model takes in the data of the wind speed and pitch angle and accordingly delivers the mechanical torque output of the turbine. This is coupled to the permanent magnet synchronous machine available in the RSCAD library representing the wind generator. The stator winding of the generator feeds power to the universal two level three phase AC-DC converter model. The controlling action of this converter is already explained in the previous section. The universal dual active bridge model is used to represent the isolated DC-DC converter. To test the correctness of the model, first the system is operated at rated conditions to confirm the proper operations of the converters. Fig. 6 shows the simulation results at the rated conditions. Fig. 6 (a)-(d) shows the MSC internal phase voltage, HVDC grid voltage, DC link voltage and power injected to the

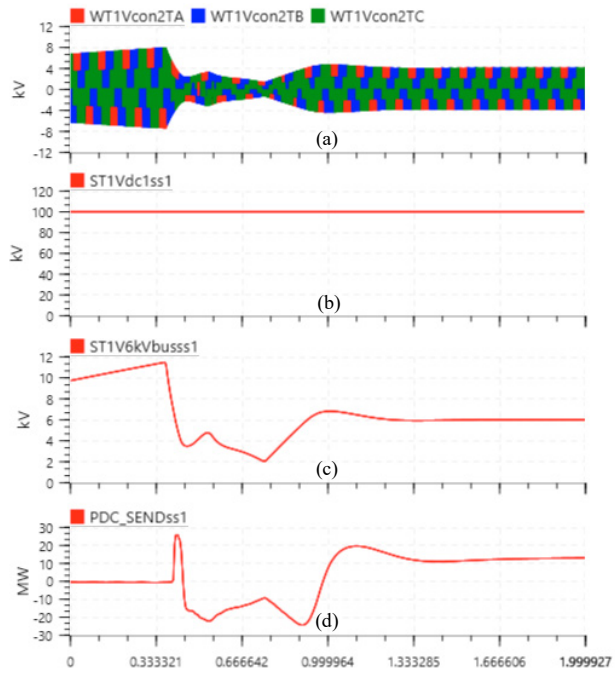

Fig. 6. Simulation at rated conditions. (a) MSC Internal Phase Voltage. (b) HVDC Grid Voltage. (c) DC Link Voltage. (d) Power Injected to the HVDC Grid.

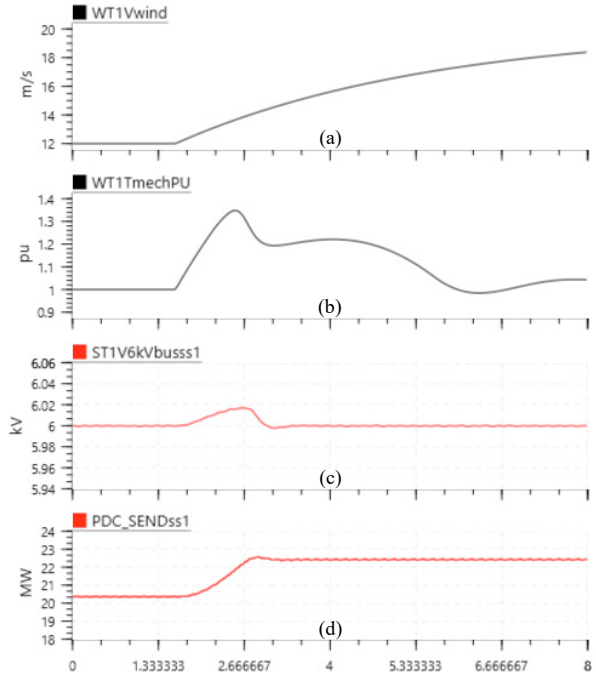

Fig. 7. Simulation results for increase in wind speed. (a) Wind Speed. (b) Mechanical Power Output of the Wind Turbine. (c) DC link Voltage. (d) Power Injected to the HVDC Grid.

HVDC grid, respectively. Initially the MSC is turned on followed by the GSC i.e. the isolated DC-DC converter. After some initial oscillation, the DC link voltage settles to the desired level of 6 KV and the power injected settles to 20 MW.

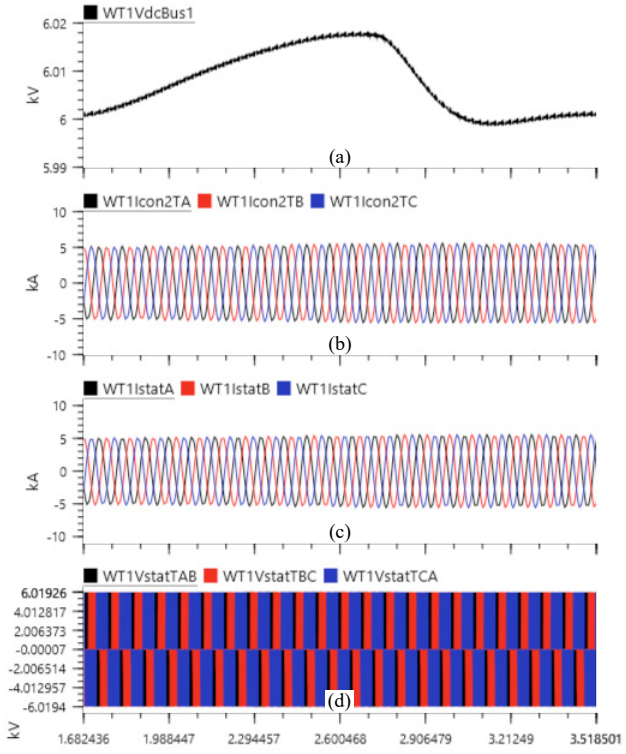

Fig. 8. Waveforms during increase in wind speed. (a) DC Link Voltage. (b) MSC Converter Currents. (c) Generator Stator Currents. (d) Generator Stator Phase Voltages.

Next, the system, is subjected to a wind speed change from 12 m/s to 20 m/s. The results are furnished in Fig. 7. Fig. 7 (a)-(d) shows the wind speed, p.u. mechanical power output of the wind turbine, DC link voltage and power injected to the HVDC grid, respectively. It is observed that as the wind speed increases, the mechanical power output of the wind turbine increases and there is a corresponding increase in the power injected to the HVDC grid. The converter is however able to maintain the DC link voltage constant at 6 kV. This validates the operation of the proposed system.

Fig. 8 shows the voltage and current waveforms during the disturbance encountered during the increase of wind speed. While the DC link voltage quickly settles to the reference with a slight momentary deviation (Fig. 8 (a)), there is an increase in the MSC converter currents and generator stator winding currents. These are shown in Fig. 8 (b) and (c), respectively. Fig. 8 (d) shows the stator winding voltages of the PMSG. These do not change with the increase with wind speed. Thus, while the AC and DC voltages are maintained, the increase in current observed leads to the increased power injection.

The system is also subjected to a decrease in wind speed and the simulation results are given in Fig. 9. The wind speed is decreased from 12 m/s to 8 m/s. A corresponding decrease in mechanical power and electrical power injection is observed. The power injected to the grid decreases to 5.7 MW. However, the isolated DC-DC converter maintains the DC link voltage at 6 kV.This further verifies the correctness of the model developed.

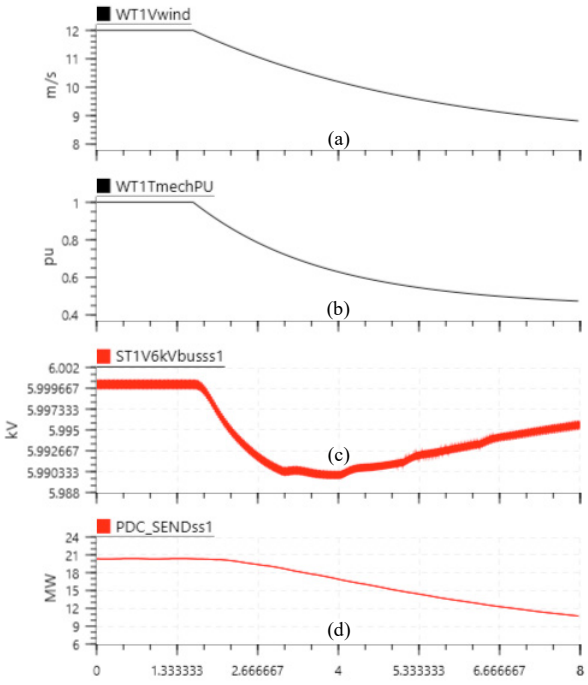

Fig. 9. Simulation results for decrease in wind speed. (a) Wind Speed. (b) Mechanical Power Output of the Wind Turbine. (c) DC link Voltage. (d) Power Injected to the HVDC Grid.

5. CONCLUSION

This paper presents an RTDS simulation model of a 20 MW HVDC wind turbine. Unlike the conventional systems which use a back-to-back converter for extracting electrical power from the wind turbine, the proposed system uses an isolated DC-DC converter after the AC-DC conversion stage to deliver power suitable for injection to HVDC grid. Such a system helps to eliminate additional system components which in turn reduces the size, weight and cost of the overall system. The simulation results furnished validates the correctness of the model. The paper presents the initial design and analysis of a technology that can be used to create large off-shore wind energy projects. In the future, the authors plan to develop a HVDC network with multiple such wind generating systems to transmit powers in the GW range to the shore from off-shore locations.

REFERENCES

.

Beig, A.R. and Muyeen, S. (2016). 4 - wind energy. In M.H. Rashid (ed.), *Electric Renewable Energy Systems*, 60–77. Academic Press, Boston. .

Blain, L. (2023). World's largest wind turbine is now fully operational and connected. .

Chuangpishit, S., Tabesh, A., Moradi-Shahrbabak, Z., and Saeedifard, M. (2014). Topology design for collector systems of offshore wind farms with pure dc power systems. *IEEE Trans. Ind. Electron.*, 61(1), 320–328. .

De Prada Gil, M., Domínguez-García, J., Díaz-González, F., Aragüés-Peñalba, M., and Gomis-Bellmunt, O. (2015). Feasibility analysis of offshore wind power plants with dc collection grid. *Renew. Energy*, 78, 467–477. .

ENTSO-E (2024). TEN-E Offshore Priority Corridor: Northern Seas Offshore Grids. Technical report, .

ENTSO-E (Jan., 2024). Offshore Network Development Plans European Offshore Network - Transmission Infrastructure Needs. Technical report, .

Fennell, E. (2018). *Comparison of On-shore and Off-shore Boundary Layers in the HARMONIE Model for Wind Energy Purposes*. Master's thesis, Wageningen University Research, .

Follo, A., Saborío-Romano, O., Tedeschi, E., and Cutululis, N.A. (2021). Challenges in all-dc offshore wind power plants. *Energies*, 14(19). .

Guan, M. (2019). A series-connected offshore wind farm based on modular dual-active-bridge (dab) isolated dc–dc converter. *IEEE Trans. Energy Convers.*, 34(3), 1422–1431. .

Honarbari, A., Najafi-Shad, S., Saffari Pour, M., Ajarostaghi, S.S.M., and Hassannia, A. (2021). Mppt improvement for pmsg-based wind turbines using extended kalman filter and fuzzy control system. *Energies*, 14(22). .

Kusiak, A., Zheng, H., and Song, Z. (2009). On-line monitoring of power curves. *Renewable Energy*, 34(6), 1487–1493. .

Li, Z., Han, H., Wang, H., and Feng, Q. (2023). Grid-connected adaptive analysis and control of the dc wind turbine under the grid-side transient faults. *IEEE Access*, 11, 129340–129352. .

Misyris, G., Van Cutsem, T., Møller, J., Dijokas, M., Estragués, O.R., Bastin, B., Chatzivasileiadis, S., Nielsen, A., Weckesser, T., Østergaard, J., and et al. (2020). North sea wind power hub: System configurations, grid implementation and techno-economic assessment. .

Nehls, G. (2023). Mingyangnbsp;reveals 18-mw offshore wind turbine model with 140-meter-long blades. .

Poynter, C. (2021). High-power offshore wind turbines need medium-voltage converter systems. .

Proctor, D. (2023). Swedish offshore wind farm could use 30-mw turbines. .

Richard, C. (2021). Plans for 1gw-plus offshore wind farm with 20mw turbines. .

Rik W. DeDoncker, Mustansir H. Kheraluwala, D.M.D. (1989). Power conversion apparatus for dc/dc conversion using dual active bridges. U.S. Patent US5027264A. .

Rodríguez, A., Vázquez, A., Lamar, D.G., Hernando, M.M., and Sebastián, J. (2015). Different purpose design strategies and techniques to improve the performance of a dual active bridge with phase-shift control. *IEEE Trans. Power Electron.*, 30(2), 790–804. .

Ryndzionek, R. and Sienkiewicz, (2020). Evolution of the hvdc link connecting offshore wind farms to onshore power systems. *Energies*, 13(8). .

Shepard, J. (2020). .

Tiku, D. (2014). dc power transmission: Mercury-arc to thyristor hvdc valves [history]. *IEEE Power and Energy Magazine*, 12(2), 76–96. .

Yuan, X. (2014). A set of multilevel modular medium-voltage high power converters for 10-mw wind turbines. *IEEE Trans. Sustain. Energy*, 5(2), 524–534. .

Yuan, X., Zhang, Y., and Peng, X. (2022). Power converter technologies for 20mw wind turbines. In *2022 IEEE Energy Convers. Congr. Expo. (ECCE)*, 1–8. .